Determination of outer molecular orbitals by collisional ionization experiments and comparison with Hartree-Fock, Kohn-Sham, and Dyson orbitals

Masakazu Yamazaki, Takuya Horio, Naoki Kishimoto, and Koichi Ohno*
Department of Chemistry, Graduate School of Science, Tohoku University, Aramaki, Aoba-ku, Sendai 980-8578, Japan
(Received 8 April 2006; revised manuscript received 17 January 2007; published 28 March 2007)

Although the outer shapes of molecular orbitals (MO's) are of great importance in many phenomena, they have been difficult to be probed by experiments. Here we show that metastable helium (He^*) atoms can sensitively probe the outer properties of molecules and that an electron spectroscopic technique using velocity-selected He^* atoms in combination with classical trajectory simulations leads to a consistent determination of MO functions and the molecular surface. MO functions composed of linear combinations of atomic orbital functions were fitted to the observed collision energy dependences of partial ionization cross sections (CEDPICS). The obtained CEDPICS MO functions were compared with conventionally available Hartree-Fock, Kohn-Sham, and Dyson orbitals.

DOI: 10.1103/PhysRevA.75.032721 PACS number(s): 34.50.Gb, 34.20.Gj

I. INTRODUCTION

The concept of molecular orbitals (MO's) plays a central role in understanding molecular structures and chemical reactivity. Its importance has been supported by successful applications of quantum chemical methods to explain a variety of experimental results. Although MO's are introduced on purely theoretical grounds, it has been an interesting subject [1] whether MO functions can be determined by experimental studies. In recent years, the observation of MO shape has been attempted by several methods. The electron diffraction technique combined with x-ray diffraction has first revealed *d*-orbital holes in copper oxide [2], and scanning tunneling microscopy (STM) has been used to visualize distorted orbitals on a solid surface [3]. For isolated molecules, electron momentum spectroscopy (EMS) [4,5] is used to image MO densities in momentum space. High-harmonic generation in an intense laser field was utilized for visualizing the highest occupied MO of N_2 [6]. A few experimental attempts have also been made for fitting the MO shape to the momentum distributions of EMS [5] or the ionization intensities of two-dimensional zero-kinetic-energy (ZEKE) photoelectron spectroscopy [7].

It is an interesting problem to compare the shape of fitted MO's to an experimental data set with those of calculated MO's in various levels of theory, such as Hartree-Fock (HF) orbitals in a single determinant self-consistent-field (SCF) theory (*ab initio* method) [8], Kohn-Sham (KS) orbitals in the density functional theory (DFT) method [9,10], and Dyson orbitals for ionization processes [11–13]. These theoretical MO's are expected to show more or less different electron distributions from each other, especially in their radial dependence at long distances from molecules. However, a comparison of an experimentally fitted MO set with theoretical MO's (SCF MO's by the HF and KS methods and Dyson orbitals) has been difficult due to a limited experimental resolution for obtaining a spatial extent of orbitals or radial behavior of transition probabilities.

Here we wish to report the determination of MO functions by atomic collision experiments. Different from other methods using photons or electrons, ionization of molecules by collisions with excited atoms in a metastable state such as $He^*(2\,^3S)$ is an excellent technique to probe the outer properties of molecules (properties in the region far from nuclei), which are of great importance in many aspects of chemical and physical phenomena that occur when a molecule contacts with other species.

When a molecule (M) collides with a $He^*(2\,^3S)$ atom, an electron transfer process can occur to yield an ion of M (M_i^+) and the ground-state He atom together with an ejected electron (e^-);

$$He^*(2\,^3S) + M \rightarrow He + M_i^+ + e^-, \tag{1}$$

where i stands for a specific ionic state of M which can be accessible with the excitation energy of He (19.82 eV). This process is known as Penning ionization [14] in which analysis of the kinetic energies (E_e) of the ejected electrons gives Penning ionization electron spectra (PIES) [15–18]. Penning ionization probabilities are shown to be strongly governed by the overlap between the He 1*s* orbital and the MO to be ionized [19,20], based on the fact that Penning ionization is considered as a two-electron rearranging process [21,22], where an electron of M is transferred into the 1*s* orbital (χ_{1s}) of He and the electron in the excited 2*s* orbital (χ_{2s}) of He^* is ejected to continuum (φ_ε). Since Penning ionization is triggered by collisions, a potential energy surface V^* between a He^* atom and M also plays a crucial role for the ionization probability. Because of a strong repulsive force between a He^* atom and M, the outer part of MO's is probed sensitively in Penning ionization. Therefore, the outer orbital of M is easily ionized, whereas the inner orbital is not, reflecting the magnitude of the overlap with the He 1*s* orbital [19,20]. It is noted that the V^* represents the target molecular surface which can be defined as minimum distances between He^* and M as a function of the collision energy (E_c) and that the change of the molecular surface with E_c leads to the change of effective overlaps between the He 1*s* orbital and the target MO's.

*Electronic address: ohnok@qpcrkk.chem.tohoku.ac.jp

When the molecular surface is soft against He^*, the larger the E_c becomes, the deeper the electron density can be probed, and hence the ionization cross section (σ) increases rapidly with the E_c. On the other hand, for the hard molecular surface, only a small increase of the ionization cross section occurs with the increase of the E_c. Niehaus formulated the collision energy dependence of Penning ionization cross sections for atomic targets on the basis of classical collision theory [16]. When a weak long-range attractive interaction can be negligible to describe the collision dynamics, the slope m of $\log(\sigma)$ vs $\log(E_c)$ is expressed by $m=B/D-1/2$, provided that the dependences on the internuclear distance R for the ionization probability $\Gamma(R)$ and the interaction potential $V^*(R)$ are of the type $\Gamma(R)=A\exp(-BR)$ and $V^*(R)=C\exp(-DR)$, respectively [16]. Therefore, as the repulsive wall of the interaction becomes harder (large D), the collision energy dependence of the ionization cross section becomes weaker (small m). In the case of molecular targets, the collision energy dependence of Penning ionization cross sections (CEDPICS) [23,24] for individual ionic states corresponding to target molecular orbitals can be obtained by two-dimensional Penning ionization electron spectroscopy [25,26], and the slope of CEDPICS often depends on the ionic states because of anisotropy of Γ and V^*.

A recent experimental improvement has made it possible to detect state-resolved electrons as a function of the time of flight of He^* by using both a sufficiently strong He^* beam source (1.6×10^{15} atoms s^{-1} sr^{-1}) [24] and a liquid nitrogen cooling to control the velocity distributions [27]. According to the theories on Penning ionization [28], CEDPICS can be computed with ionization probabilities $\Gamma^{(i)}$ and interaction potentials V^* combined with classical trajectory simulations [29,30]. It follows that simulations based on the theoretical model so as to obtain a good agreement with the observation by a new experimental apparatus [27] lead to consistent experimental determination of MO functions (ionization probabilities), and the molecular surface (V^* functions).

II. METHODS

A. Ionization widths

According to the golden rule formula of Penning ionization [31], the ionization width $\Gamma^{(i)}$ for producing the ith ionic state of M is given by

$$\Gamma^{(i)}=2\pi\rho^{(i)}|\langle\Phi_0|V|\Phi^{(i)}\rangle|^2, \tag{2}$$

where $\rho^{(i)}$ is the density of final states that is related to a normalization of the continuum wave function, V is the electronic Hamiltonian (actually, $1/r_{12}$), and Φ_0 and $\Phi^{(i)}$ are the electronic wave functions for the initial (He^*+M) and final ($He+M_i^+ + e^-$) states, respectively. The wave functions for the system can be given as products of the wave functions of M (Ψ_0^N for the neutral ground state with N electrons, Ψ_i^{N-1} for the ith cationic state with $(N-1)$ electrons, the He atom (ψ_{He^*} for the excited state, ψ_{He} for the ground state), and the ejected electron (φ_ε),

$$\Phi_0=\Psi_0^N\psi_{He^*}, \tag{3}$$

$$\Phi^{(i)}=\Psi_i^{N-1}\psi_{He}\varphi_\varepsilon. \tag{4}$$

The matrix element of Eq. (2) thus can be expressed as

$$\langle\Phi_0|V|\Phi^{(i)}\rangle\approx\langle\Psi_0^N\psi_{He^*}|V|\Psi_i^{N-1}\psi_{He}\varphi_\varepsilon\rangle. \tag{5}$$

Penning ionization is considered as a two-electron rearranging process [21,22], where an electron of M is transferred into the $1s$ orbital (χ_{1s}) of He, and the electron in the excited $2s$ orbital (χ_{2s}) of He^* is ejected to the continuum (φ_ε). Based on well-established treatments for electron transfer rates [32] and MO theories [33], a two-electron exchange integral can be converted into the product of overlap integrals,

$$\langle\Phi_0|V|\Phi^{(i)}\rangle\approx\langle\Psi_0^N|\Psi_i^{N-1}\chi_{1s}\rangle\langle\chi_{2s}|\varphi_\varepsilon\rangle, \tag{6}$$

where the overlap between the neutral and ith cationic wave functions of M, $\langle\Psi_0^N|\Psi_i^{N-1}\rangle$, can be denoted as a Dyson orbital ϕ_i^{Dyson} [11] and Eq. (6) is thus rewritten as

$$\langle\Phi_0|V|\Phi^{(i)}\rangle\approx\langle\phi_i^{\text{Dyson}}|\chi_{1s}\rangle\langle\chi_{2s}|\varphi_\varepsilon\rangle. \tag{7}$$

It is of note that the ionization width $\Gamma^{(i)}(\mathbf{R})$ of Penning ionization for molecular targets depends on the relative orientation $\mathbf{R}$ of M to a He^* atom, since the magnitude of overlap integrals in Eq. (7) is a function of the position of He^*. However, as discussed by Miller and Morgner [22], the overlap between the He^* $2s$ and continuum orbitals ($\langle\chi_{2s}|\varphi_\varepsilon\rangle$) does not strongly depend on the position of He^*, and it can be replaced by a scaling factor. Thus, the ionization probability producing the ith ionic state of M can be evaluated by the overlap between the $1s$ orbital of He and an orbital of M to be ionized,

$$\Gamma^{(i)}=k^{(i)}|\langle\phi_i^{\text{Dyson}}|\chi_{1s}\rangle|^2, \tag{8}$$

where $k^{(i)}=2\pi\rho^{(i)}|\langle\chi_{2s}|\varphi_\varepsilon\rangle|^2$ is a parameter to be determined in order to reproduce experimental branching ratios. It should be noted that the Dyson orbital ($\phi_i^{\text{Dyson}}=\langle\Psi_0^N|\Psi_i^{N-1}\rangle$) is defined by the exact wave functions for both the neutral and ionic states. It follows that the Dyson orbital is a one-electron orbital without approximation, whereas a conventional SCF MO in the HF (*ab initio*) or the KS (DFT) scheme will appear in Eq. (8) ($\Gamma^{(i)}=k^{(i)}|\langle\phi_i^{\text{HF}}|\chi_{1s}\rangle|^2$ or $\Gamma^{(i)}=k^{(i)}|\langle\phi_i^{\text{KS}}|\chi_{1s}\rangle|^2$) if the approximate wave functions for M and M_i^+ are used in Eq. (5).

B. Classical trajectory calculations

In the present study, the classical trajectory method was used for simulations of CEDPICS. The ionization cross section $\sigma^{(i)}$ for producing the ith ionic state of M can be obtained as a function of E_c by the following equation with an averaged ionization probability $\overline{P_{\mathbf{\Omega},\mathbf{L}}^{(i)}}$:

$$\sigma^{(i)}(E_c)=\int 2\pi b\overline{P_{\mathbf{\Omega},\mathbf{L}}^{(i)}}(b;E_c)db. \tag{9}$$

Here, at a given collision energy E_c, initial conditions for the impact parameter b, the molecular orientation $\mathbf{\Omega}$, and the direction of the angular momentum vector $\mathbf{L}$ are randomly

generated. Since the ionization probability for molecular collisions depends not only on b but also on molecular orientation ($\mathbf{\Omega}$) and rotation ($\mathbf{L}$), it should be averaged over them to give the collision energy dependence of the ionization cross section $\sigma^{(i)}(E_c)$.

In each trajectory with a set of initial conditions (E_c, b, $\mathbf{\Omega}$, $\mathbf{L}$, etc.), physical quantities can be expressed as a function of time t. The time evolution of the relative motion between the center of mass of M and the He^* atom is determined by the equations of motion, in which the intermolecular forces are evaluated by the gradients of the interaction potential functions V^*. Therefore, CEDPICS is a functional of both $\Gamma^{(i)}$ and V^*. The partial ionization probability $P^{(i)}$ with specific b and E_c can be determined by integration of the partial ionization probability in a time interval dt, $\frac{\Gamma^{(i)}(\mathbf{r}(t))}{\hbar}dt$, over a whole span of t,

$$P^{(i)} = \int_0^\infty S(t)\frac{\Gamma^{(i)}(\mathbf{r}(t))}{\hbar}dt, \tag{10}$$

where a statistical survival factor $S(t)$ for the metastable He atom at a particular time t can be estimated by using the integrated total ionization probabilities $\Sigma_i P_{\text{int}}^{(i)}$ before time t $[S(t)=1-\Sigma_i P_{\text{int}}^{(i)}]$. By changing initial collision energy E_c, theoretical CEDPICS can be obtained by the classical trajectory calculations.

C. Optimizations

As an initial guess of MO functions used for estimations of $\Gamma^{(i)}$, SCF MO's with the minimal basis set were used, and the optimization was performed under a double-ζ framework. Therefore, the MO functions to be determined were expressed by a linear combination of atomic orbitals χ (LCAO),

$$\phi_i = \sum_p^M C_{ip}\chi_p + \sum_q^M C_{iq}\chi_q, \tag{11}$$

where the basis set χ is the Slater-type orbital expanded by six Gaussian-type orbitals. The LCAO expansion coefficients and the basis set exponents were set to be variable parameters for ϕ_i. The parameter fit for ϕ_i is constrained by the orthonormality condition and the conservation of orbital symmetries.

In order to perform efficient optimization of V^*, a suitable initial guess of V^* is required. Since interaction potentials are mainly related to the outermost electrons, one electron addition into the $1s$ vacancy leads to the use of a $Li(2\,^2S)$ atom in place of a $He^*(2\,^3S)$ atom to obtain crude interaction potentials V_{Li}. This Li model is reasonable as an initial guess, because the resemblance between a $Li(2\,^2S)$ atom and a $He^*(2\,^3S)$ atom has been confirmed by many experimental studies [34–38]. On this basis, the *ab initio* Li model potential energy surface $V_{Li}(r,\theta)$ calculated by using a $Li(2\,^2S)$ was then modified with correction terms. Since the interactions between atoms and molecules are essentially governed by the overlap between wave functions, the correction terms were introduced with an exponential function [39]

$$\begin{aligned} V^*(r,\theta) &= V_{Li}(r,\theta) + \text{correction terms} \\ &= V_{Li}(r,\theta) + \exp(-r/B)\sum_{l=0}^{2} A_l P_l(\cos\theta), \end{aligned} \tag{12}$$

where anisotropic correction was expressed by Legendre polynomials $P_l(\cos\theta)$. Exponent B and Legendre expansion coefficients A_l were set to be parameters for V^*.

A nonlinear least-squares fitting method was employed, where V^* and ϕ_i are modified in order to minimize the following residue χ^2:

$$\chi^2 = \sum_{i,E_c} w^{(i)}(E_c)[\sigma_{\text{expt}}^{(i)}(E_c) - \sigma_{\text{calc}}^{(i)}(E_c)]^2, \tag{13}$$

where $\sigma_{\text{expt}}^{(i)}(E_c)$ and $\sigma_{\text{calc}}^{(i)}(E_c)$ are observed and calculated partial Penning ionization cross sections as a function of E_c, respectively, and i represents ionic states, and a weighting factor $w^{(i)}(E_c)$ associates with experimental errors. The optimization step was determined by the modified Marquardt method [40], and the gradient vector and the Hessian matrix for obtaining the step were updated based on the hybrid method proposed by Powell [41]. By changing the $k^{(i)}$ parameters [Eq. (8)] and the parameters for ϕ_i [Eq. (11)] and V^* [Eq. (12)], the trajectory simulations for CEDPICS were repeated in order to minimize Eq. (13).

III. RESULTS AND DISCUSSION

Figure 1 shows CEDPICS for N_2 by collision with $He^*(2\,^3S)$ atoms, in which experimental CEDPICS with a wide E_c range (E_c=20–300 meV) was taken from Ref. [27]. Ionic states $X(^2\Sigma_g^+)$, $A(^2\Pi_u)$, and $B(^2\Sigma_u^+)$, produced for $N_2+He^*(2\,^3S)$, are assigned to one-electron removal from the $3\sigma_g$, $1\pi_u$, and $2\sigma_u$ MO's of N_2, respectively. Different E_c dependences of the ionization cross sections reflect the interaction potentials around different parts (collinear or perpendicular directions to the molecular axis) of a nitrogen molecule depending on the electron distributions of the corresponding MO's [24,30]. The ionization cross section for the $^2\Pi_u$ state most rapidly increases as an increase of E_c. The CEDPICS for the remaining two Σ states also show significantly different behavior from each other, especially in the lower-E_c range. The dashed lines in Fig. 1 represent the initial guess before optimization, where the SCF MO's with the minimal basis and the Li-model interaction potential V_{Li} were used for the simulations. As shown by solid lines, simulated CEDPICS with optimized MO's (CEDPICS MO's) and V^* fit well with experimental CEDPICS in the whole E_c range.

In Fig. 2(a), potential energy is shown as contours for arbitrary positions of a ground-state He atom (V_{He}), of a metastable He^* $(2\,^3S)$ atom (V_{He^*}), and of a ground-state Li $(2\,^2S)$ atom (V_{Li}) against a N_2 molecule. Depending on the MO distributions, σ and π orbitals are effectively ionized when a He^* atom approaches the collinear and perpendicular directions of the molecular axis, respectively. Table I lists optimized parameters for V^* in Eq. (12) and $k^{(i)}$ for ionization widths in Eq. (8). Since interaction potentials are mainly

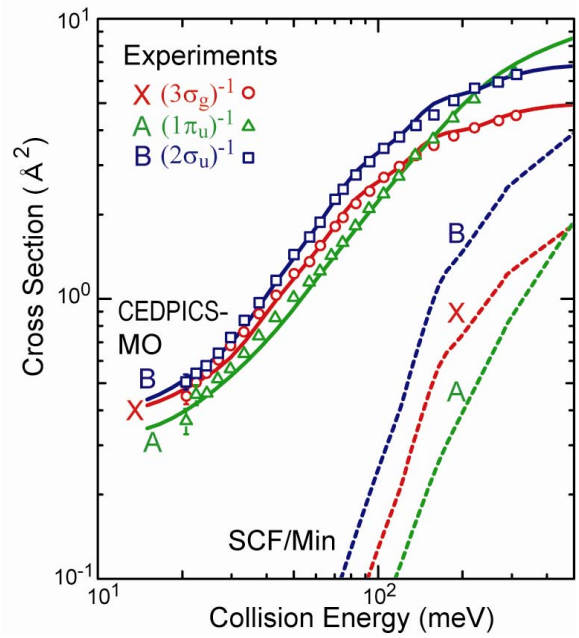

FIG. 1. (Color online) Observed and simulated collision energy dependence of Penning ionization cross sections (CEDPICS) for N_2+He*(2 ^3S). Observed partial cross section for *X* (circle), *A* (triangle), and *B* (square) states. Experimental statistical errors are as large as the size of the markers except for the edge of the low-collision-energy side. Simulated CEDPICS are drawn with solid or dashed lines by using optimized MO's in a valence double-ζ-type basis (CEDPICS MO) and SCF MO's in the minimal basis set (SCF-Min), respectively.

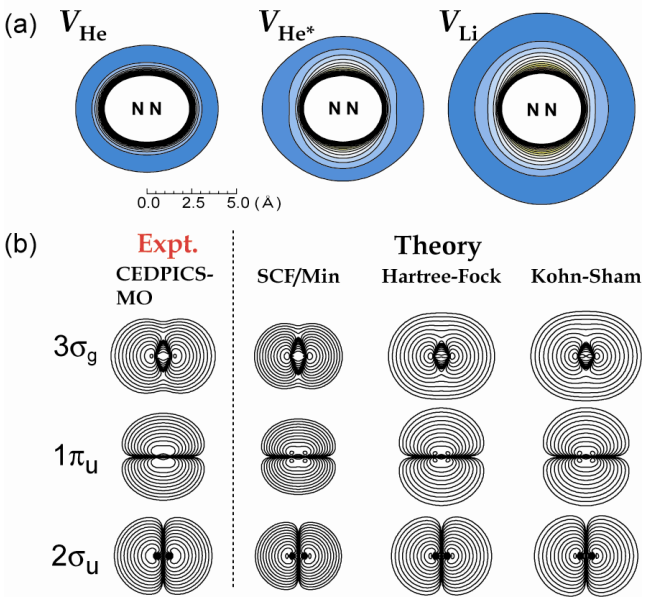

FIG. 2. (Color online) (a) The contour map of the potential energy surface around a N_2 molecule in interaction with various atomic probes. The energy spacing is 50 meV from 0 meV to 800 meV. V_{He} and V_{Li} were calculated by CCSD(T)/6-311+G*. (b) Electron density contour maps for various MO's corresponding to the observed three ionic states for N_2. The density of the *n*th contour line increases from the outermost value of 1.0×10^{-7} a.u.$^{-3}$ with a proportionality constant of 4^{n-1}.

governed by the outermost electrons, the interaction potentials with the ground-state He atom should be considerably different from those with the He*(2 ^3S) atom. The experimental V_{He^*} is really remarkably different from the calculated V_{He} for the ground-state He atom, whereas it is rather similar to V_{Li}, because the outermost 2*s* electron of He* or Li governs the interaction potential in both cases. The obtained V_{He^*} in Fig. 2(a) demonstrates the resemblance between He* and Li atoms proposed in earlier studies [34–38].

As can be seen from the optimized parameters listed in Table I a significant difference between V_{He^*} and V_{Li} should be noticed. Since the present CCSD(T) calculations for V_{Li} cannot completely take electron correlations into account, the lack of electron correlation in V_{Li} was made up for in the negative isotropic correction term (A_0=−1360 meV). The anisotropic correction term A_2=393 meV reduces the interaction energy in the perpendicular directions to the molecular axis more than in the collinear directions. This indicates that the interaction between He* 2*s* and unoccupied π^* orbitals of N_2 is responsible for the dominant contributions in the corrections, since He*(2 ^3S) has a shallower 2*s* orbital energy than Li. Furthermore, the optimized value (1.016 Å) of the *B* parameter is comparable to the order of exponential decay for unoccupied MO's rather than occupied MO's. Comparison of ionization potentials (He*, 4.768 eV; Li, 5.392 eV) and 2*s*-2*p* energy gaps (He*, 1.144 eV; Li, 1.848 eV) between He*(2 ^3S) and Li(2 ^2S) can explain the considerable reduction of the sizes of the molecular surface from V_{Li} to V_{He^*}, which is consistent with a previous study [30].

The optimized $k^{(i)}$ parameters in Table I show a consistent trend to previous studies [30,39]; the larger the ionization energy becomes (the smaller the kinetic energy of ejected electron E_e), the larger the respective $k^{(i)}$ parameter is ($k^{(X)}<k^{(A)}<k^{(B)}$). This tendency is at least partly due to the density of final states $\rho^{(i)}$ in Eq. (2) ($k^{(i)}=2\pi\rho^{(i)}|\langle\chi_{2s}|\varphi_\varepsilon\rangle|^2$). With a normalization of the Coulomb radial function for ejected electrons, the density of final continuum states becomes $2\pi\rho^{(i)}=4/\sqrt{2E_e}$ in a.u. [42]. Moreover, the energy gap between the He 1*s* orbital and the target ionized orbital may also be responsible for this tendency. The two electron integrals related to electron transfer may have larger values when the energy gap becomes smaller, although this effect is not included in Eq. (8) after employing the Mulliken approximation [33] and is effectively included in $k^{(i)}$ parameters.

TABLE I. Optimized parameters A_l and B in the potential correction terms of $\exp(-r/B)\Sigma_{l=0}^{2}A_lP_l(\cos\theta)$ and $k^{(i)}$ parameters for ionization widths in Eq. (8).

Parameter	N_2+He*(2 ^3S)
B (Å)	1.016
A_0 (meV)	−1360
A_2 (meV)	393
$k^{(X)}$ (eV)	5.02
$k^{(A)}$ (eV)	6.66
$k^{(B)}$ (eV)	7.94

Figure 2(b) shows electron density contour maps for various MO's corresponding to the observed three ionic states for N_2. The fitted MO's (CEDPICS MO's) are compared with three types of theoretical MO's: SCF MO's with the minimal basis (SCF-Min), SCF MO's in the near-HF limit (HF), and B3LYP (KS) orbitals in DFT. By using a large basis set composed of 138-contracted Gaussian type orbitals ([7*s*6*p*4*d*2*f*] CGTO), SCF MO's in the near-HF limit were obtained. The [7*s*6*p*] CGTO of the cc-pV6Z basis was combined with the [4*d*2*f*] CGTO used in the study by Feller *et al.* [43]. KS orbitals were obtained with the same basis used for the HF calculations by using the B3LYP functional [44].

Since the electron densities of SCF-Min MO's are mainly concentrated around the nuclei, the magnitude of the overlap integral, which plays an essential role in determining CEDPICS, increases very rapidly as a $He^*(2\,^3S)$ atom approaches the shorter distances. The electron distributions of CEDPICS MO's are shown to be comparable to those of the precise theoretical MO's, although even the number of parameters to represent CEDPICS-MO (16-CGTO) is considerably (8.5 times) smaller than that of the HF and KS orbitals (138-CGTO).

In order to compare CEDPICS MO's with theoretical MO's in detail, the electron density $\rho_e^{(i)}(r)$ of individual MO's is plotted as a function of distance r from the center of mass of a N_2 molecule in Fig. 3. It is clear from Fig. 3 that the electron density of SCF-Min MO's decreases too rapidly as the increase of distance, and its behavior is considerably different from those of other MO's. Different from the SCF-Min MO's, CEDPICS MO's are comparable to more precise theoretical MO's. It should be noted that KS orbitals are more extending outside than HF orbitals, whereas CEDPICS MO's are rather more compact than HF orbitals. Figure 3 also shows the results of Dyson orbitals. The Dyson orbital for the *i*th ionic state, which is also denoted as a generalized overlap amplitude or a Feynman-Dyson amplitude, can be defined as an overlap between a neutral (N-electron system) and the respective ionic [$(N-1)$-electron system] wave functions ($\phi_i^{\mathrm{Dyson}} \equiv \langle \Psi_0^N | \Psi_i^{N-1} \rangle$). In practice, however, it is difficult to obtain reliable Dyson orbitals even by post-Hartree-Fock methods due to large orbital relaxation and electron correlation effects. In order to take electron correlations into account for the wave functions, symmetry-adapted cluster (SAC) and SAC-CI methods [45,46] were used in this study to compute approximate Dyson orbitals for N_2 with the basis sets of cc-pV5Z, which was shown to take electron correlations effectively and resulted in better total energy than the [7*s*6*p*4*d*2*f*] CGTO basis used to calculate HF and KS orbitals. From Fig. 3, theoretical Dyson orbitals are found to be rather more spatially compact than the HF orbitals. This propensity agrees with that of CEDPICS MO's, and it is consistent with the fact that the pole strength in the outer valence Green's function method [13], which is related to the probability associated with Koopmans' picture, is always smaller than unity.

The difference in the radial dependence among the various MO's compared in Fig. 3 can be seen more clearly in Fig. 4, where logarithmic derivatives of MO electron densities are shown. It is well known that the electron densities of

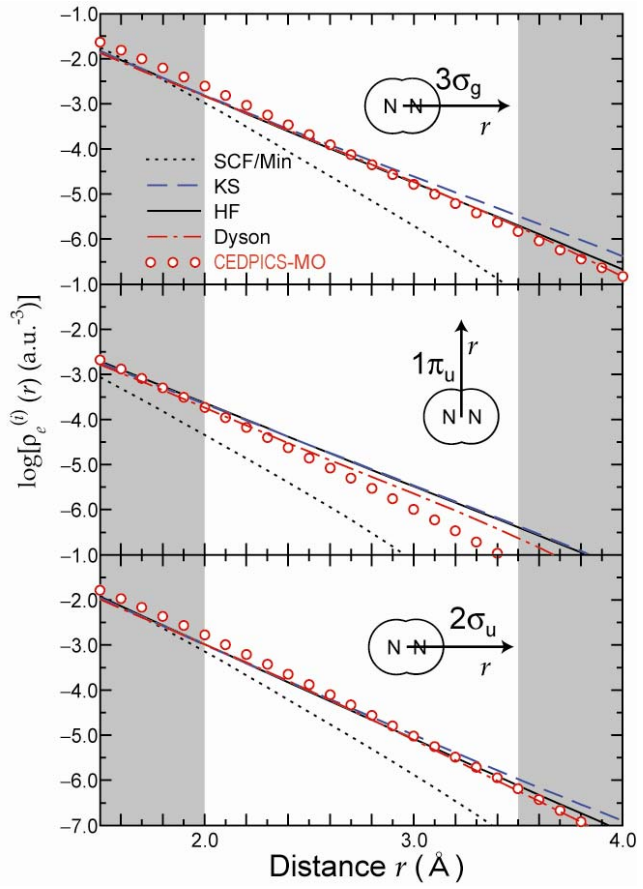

FIG. 3. (Color online) Electron density of various kinds of MO's for N_2 as a function of distance r from the center of N_2. The directions are collinear and perpendicular to the molecular axis for σ and π MO's, respectively. Optimized MO (CEDPICS MO, circle), and theoretical MO's, Hartree-Fock (HF: solid line), Kohn-Sham (KS: long dashed line), SCF with the minimal basis (dotted line), and Dyson orbitals with cc-pV5Z (chained line) basis sets are shown. Shades represent less reliable regions in the collision experiments.

all HF orbitals decay at long distance as an exponential function in which the exponent is determined by the orbital energy of the highest occupied MO (HOMO) $\varepsilon_{\mathrm{HOMO}}$ [47–49],

$$\rho_e^{(i)}(r) = |\phi_i(r)|^2 \sim \exp(-2\alpha_0 r), \alpha_0 = (-2\varepsilon_{\mathrm{HOMO}})^{1/2}, \tag{14}$$

where r is the distance from the center of a nitrogen molecule. The behavior of the decay parameter -2α can be checked from a logarithmic derivative of the electron density, $\frac{d[\ln \rho_e^{(i)}(r)]}{dr}$. Table II shows average values of -2α for CEDPICS MO's and calculated MO's in which they were evaluated within the regions from 2.0 Å to 3.5 Å in Fig. 4. According to Eq. (14) with $\varepsilon_{\mathrm{HOMO}}=-0.61415$ a.u. calculated in the present study, the decay parameters of all three HF SCF orbitals of N_2 (solid line) should converge to $-2\alpha_0=-2(-2\varepsilon_{\mathrm{HOMO}})^{1/2}=-2.22$ a.u.$^{1/2}$ at long range. The -2α of the present HF orbitals in Fig. 4 is almost constant in the wide range of the distance r, and the obtained average values are slightly smaller than $-2\alpha_0$ (=−2.22 a.u.$^{1/2}$). The

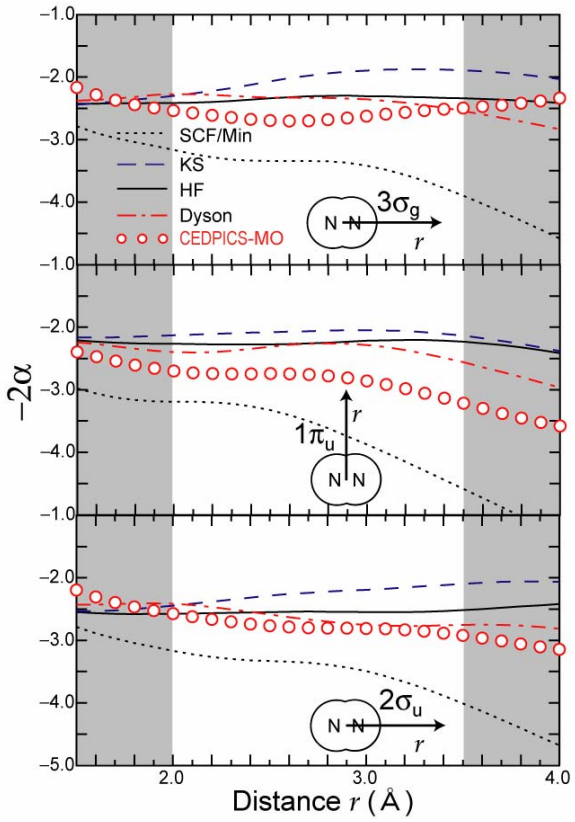

FIG. 4. (Color online) The logarithmic derivative of electron densities, -2α, for various kinds of MO's as a function of distance r.

KS orbitals give larger (negatively smaller) -2α values by ca. 0.3 for all ionic states than HF orbitals, and this tendency did not depend on the choice of the functionals in the DFT calculations. On the contrary, the values of -2α for theoretical Dyson orbitals are rather smaller than the asymptotic value of HF orbitals, $-2\alpha_0$. For CEDPICS MO's, the -2α values are significantly smaller than $-2\alpha_0$.

From Table II and Fig. 4, a state dependence of -2α values can be noticed. The -2α values for CEDPICS MO's clearly depend on the ionic states, and its tendency was dramatically changed from those of the original SCF-Min orbitals. It should be noted here that the A state of CEDPICS MO's shows the smallest -2α value (−2.85) among the ionic states presented in Table II. However, for Penning ionization, the most effective distance is often different for σ and π orbitals due to the anisotropic change in molecular surface. From trajectory analysis, the effective region for the A state is from 2.0 Å to 3.0 Å where the averaged -2α value for the π orbital of CEDPICS MO's is −2.76 a.u.$^{1/2}$. From this consideration, the -2α value for the A state of CEDPICS MO's is thus between X and B states.

For the calculated MO's (HF, KS, and Dyson orbitals), the -2α values for the B state slightly deviate from those for other states (X and A). For Dyson orbitals, the state dependence of -2α was studied by Morrison *et al.* [51]. They found from expensive computations that each Dyson orbital corresponding to the ionic states of Li ($^{1,3}S$, $^{1,3}P$, and $^{1,3}D$) has its own characteristic radial behavior determined by the respective ionization energy I_i (it is noted that I_i is also an eigenvalue of each Dyson orbital) [51]. By using the observed ionization energies [50], the expected decay parameters $-2\sqrt{2I_i}$ for theoretical Dyson orbitals are listed in Table II. The relationship between X and B states for the present Dyson orbitals is consistent with the prediction, but the A state shows the same -2α as the X state, which may be due to the quality of the present calculations for Dyson orbitals. However, to improve the calculated Dyson orbital shape in a secondary important region for total energy, one needs other indexes than (ionization) energy, since the present level (SAC/SAC-CI) of calculation well reproduces experimental ionization energies within 300 meV.

The previous experimental attempts [5,7] to fit electron densities of ionized MO's implied or assumed that Dyson orbital must be optimized by an experimental data set. Very recently, the theoretical treatment of high-harmonic generation in an intense laser field was extended to include many electron effects and it was reinterpreted as the molecular orbital tomography measured Dyson orbitals [52]. Kohn-Sham orbitals are often sufficient to empirically analyze experimental electron momentum distributions, which was warned of by Ning *et al.* who recently revealed a link between the electron momentum distributions (EMD's) and Dyson orbitals using an electron momentum spectroscopic study in combination with one-particle Green's function theory [53].

To study the spatial distribution of Penning ionization probabilities has some important aspects compared with other methods using photons or electrons. Nicholson *et al.* developed an inversion procedure to obtain Dyson orbitals from experimental EMS data, which relies on the validity of the plane- and distorted-wave impulse approximations [5,54]. Although they presented momentum distributions calculated by using the fitted orbitals and Hartree-Fock orbital or a double-ζ-level SCF orbital, the direct comparison of orbital shape itself between the fitted MO and the SCF MO

TABLE II. Average value[a] (in a.u.$^{1/2}$) of the logarithmic derivative of electron densities (-2α) for various MO's corresponding observed ionic states.

Method	Ionic state		
	X	A	B
SCF-Min	−3.43	−3.69	−3.47
HF	−2.34	−2.34	−2.54
KS	−2.02	−2.08	−2.25
Dyson	−2.36	−2.36	−2.64
CEDPICS	−2.61	−2.85 (−2.76)[d]	−2.77
$-2\sqrt{-2\varepsilon_{\mathrm{HOMO}}}$ $(-2\alpha_0)$[b]	−2.22	−2.22	−2.22
$-2\sqrt{2I_i}$[c]	−2.14	−2.22	−2.35

[a]-2α values (a.u.$^{1/2}$) in Fig. 4 are averaged in the regions of 2.0–3.5 Å.
[b]The asymptotic value for HF orbitals estimated by the present orbital energy.
[c]Experimental ionization energies were taken from Ref. [50].
[d]The averaged value over the effective region (2.0–3.0 Å) for the A state (see text).

was not discussed. Compared with the methods using lasers [6,7], $He^*(2\,^3S)$ with the excitation energy of 19.82 eV can ionize relatively deeper MO's. Therefore, we can obtain CEDPICS MO's for several ionic states in position space at the same time, and it becomes possible to discuss the difference in their spatial distributions.

IV. CONCLUSION

The spatial shape of the ionization widths and the interaction potential surface were first optimized simultaneously by using observed collision energy dependence of partial ionization cross sections (CEDPICS) for $He^*(2\,^3S)+N_2$. The obtained potential energy surface between $He^*(2\,^3S)$ and N_2 was consistent with previous studies. The optimization of the ionization widths was performed based on the overlap approximation in which the ionized molecular orbitals of N_2 were set to be unknown functions. The electron densities of SCF MO's with the minimal basis, which were the initial guess for the optimization, were dramatically changed by the experimental data. The spatial extent of the optimized MO's (CEDPICS MO's) is comparable to conventionally available more precise orbitals, such as Hartree-Fock, Kohn-Sham, and Dyson orbitals.

By checking the radial dependences of electron densities for the calculated MO's, the characteristic behavior of each MO was found. It is theoretically well known that HF orbitals decay at long distance as an exponential function in which the exponent is determined by the orbital energy of the HOMO. The decay parameter in the present KS orbitals showed slightly larger values, which means the electron density distributions of KS orbitals are more diffuse than those of HF orbitals. On the other hand, Dyson orbitals showed slightly smaller values than the converged decay rate $-2\alpha_0$ for the HF orbitals. CEDPICS MO's showed substantially smaller values of -2α.

Although the most rigorous description of ionized MO's is known as Dyson orbitals, it is difficult to get information on the shape of Dyson orbitals from both theory and experiment. Theoretical difficulties in obtaining the Dyson orbital shape lie in the treatments of electron correlations and orbital relaxations. Although most of the theoretical improvements are focused on eigenvalues (ionization energies), Hartree-Fock, Kohn-Sham, and Dyson orbitals are expected to show different spatial structures, such as the spatial extents of electron densities and the decay rates of the densities.

A direct comparison between an experimentally fitted MO and theoretical MO has been difficult so far, because of the complex theoretical treatment of the dynamical process and experimental resolution in the space of orbitals or transition probability. In this study, a collisional ionization experiment was first used to examine the shape of MO's within the present model of analysis.

ACKNOWLEDGMENTS

The present work was supported by a Grant-in-Aid for Scientific Research from the Japanese Ministry of Education, Culture, Sports, Science and Technology. M.Y. and T.H. are supported by the Japan Society for the Promotion of Science for Young Scientists.

[1] K. Fukui, Int. J. Quantum Chem., Quantum Chem. Symp. **12**, 277 (1977).
[2] J. M. Zuo, M. Kim, M. O'Keeffe, and J. C. H. Spence, Nature (London) **401**, 49 (1999).
[3] J. I. Pascual, J. Gómez-Herrero, C. Rogero, A. M. Baró, D. Sánchez-Portal, E. Artacho, P. Ordejón, and J. M. Soler, Chem. Phys. Lett. **321**, 78 (2000).
[4] Y. Zheng, J. J. Neville, and C. E. Brion, Science **270**, 786 (1995).
[5] E. Weigold and I. E. McCarthy, *Electron Momentum Spectroscopy* (Kluwer Academic/Plenum, New York, 1999).
[6] J. Itatani, J. Levesque, D. Zeidler, H. Niikura, H. Pepin, J. C. Kieffer, P. B. Corkum, and D. M. Villeneuve, Nature (London) **432**, 867 (2004).
[7] M. S. Ford and K. Müller-Dethlefs, Phys. Chem. Chem. Phys. **6**, 23 (2004).
[8] W. J. Hehre, L. Radom, P. v. R. Schleyer, and J. A. Pople, *Ab Initio Molecular Orbital Theory* (Wiley, New York, 1986).
[9] W. Kohn and L. J. Sham, Phys. Rev. **140**, A1133 (1965).
[10] R. G. Parr and W. Yang, *Density-functional Theory of Atoms and Molecules* (Oxford University Press, New York, 1989).
[11] O. Goscinski and P. Lindner, J. Math. Phys. **11**, 1313 (1970).
[12] L. S. Cederbaum, J. Phys. B **8**, 290 (1975).
[13] J. V. Ortiz, J. Chem. Phys. **104**, 7599 (1996).
[14] F. M. Penning, Naturwiss. **15**, 818 (1927).
[15] V. Čermák, J. Chem. Phys. **44**, 3781 (1966).
[16] A. Niehaus, Adv. Chem. Phys. **45**, 399 (1981).
[17] A. J. Yencha, *Electron Spectroscopy: Theory, Techniques, and Applications* (Academic Press, New York, 1984), Vol. 5.
[18] P. E. Siska, Rev. Mod. Phys. **65**, 337 (1993).
[19] K. Ohno, H. Mutoh, and Y. Harada, J. Am. Chem. Soc. **105**, 4555 (1983).
[20] K. Ohno, S. Matsumoto, and Y. Harada, J. Chem. Phys. **81**, 4447 (1984).
[21] H. Hotop and A. Niehaus, Z. Phys. **228**, 68 (1969).
[22] W. H. Miller and H. Morgner, J. Chem. Phys. **67**, 4923 (1977).
[23] K. Mitsuke, T. Takami, and K. Ohno, J. Chem. Phys. **91**, 1618 (1989).
[24] K. Ohno, T. Takami, K. Mitsuke, and T. Ishida, J. Chem. Phys. **94**, 2675 (1991).
[25] K. Ohno, H. Yamakado, T. Ogawa, and T. Yamata, J. Chem. Phys. **105**, 7536 (1996).
[26] K. Ohno, Bull. Chem. Soc. Jpn. **77**, 887 (2004).
[27] T. Horio, M. Yamazaki, S. Maeda, T. Hatamoto, N. Kishimoto, and K. Ohno, J. Chem. Phys. **123**, 194308 (2005).
[28] W. H. Miller, J. Chem. Phys. **52**, 3563 (1970).
[29] T. Ogawa and K. Ohno, J. Chem. Phys. **110**, 3773 (1999).
[30] S. Maeda, M. Yamazaki, N. Kishimoto, and K. Ohno, J. Chem. Phys. **120**, 781 (2004).
[31] W. H. Miller, Chem. Phys. Lett. **4**, 627 (1970).

[32] S.-I. Choi, J. Jortner, S. A. Rice, and R. Silbey, J. Chem. Phys. **41**, 3294 (1964).
[33] R. S. Mulliken, J. Chim. Phys. Phys.-Chim. Biol. **46**, 497 (1949).
[34] E. W. Rothe, R. H. Neynaber, and S. M. Trujillo, J. Chem. Phys. **42**, 3310 (1965).
[35] E. E. Muschlitz, Jr., Science **159**, 599 (1968).
[36] H. Hotop, Radiat. Res. **59**, 379 (1974).
[37] H. Haberland, Y. T. Lee, and P. E. Siska, Adv. Chem. Phys. **45**, 487 (1981).
[38] H. Hotop, T. E. Roth, M.-W. Ruf, and A. J. Yencha, Theor. Chem. Acc. **100**, 36 (1998).
[39] M. Yamazaki, S. Maeda, N. Kishimoto, and K. Ohno, Chem. Phys. Lett. **355**, 311 (2002).
[40] W. H. Press, B. P. Flannery, S. A. Teukolsky, and W. T. Vetterling, *Numerical Recipes in C* (Cambridge University Press, Cambridge, England, 1988).
[41] M. J. D. Powell, Comput. J. **7**, 155 (1964).
[42] W. H. Miller, C. A. Slocomb, and H. F. Schaefer III, J. Chem. Phys. **56**, 1347 (1972).
[43] D. Feller, C. M. Boyle, and E. R. Davidson, J. Chem. Phys. **86**, 3424 (1987).
[44] A. D. Becke, J. Chem. Phys. **98**, 5648 (1993).
[45] H. Nakatsuji, Chem. Phys. Lett. **59**, 362 (1978).
[46] H. Nakatsuji and K. Hirao, J. Chem. Phys. **68**, 2053 (1978).
[47] N. C. Handy, M. T. Marron, and H. J. Silverstone, Phys. Rev. **180**, 45 (1969).
[48] M. M. Morrell, R. G. Parr, and M. Levy, J. Chem. Phys. **62**, 549 (1975).
[49] J. Katriel and E. R. Davidson, Proc. Natl. Acad. Sci. U.S.A. **77**, 4403 (1980).
[50] K. Kimura, S. Katsumata, Y. Achiba, T. Yamazaki, and S. Iwata, *Handbook of He I Photoelectron Spectra of Fundamental Organic Molecules* (Japan Scientific, Tokyo, 1981).
[51] R. C. Morrison, J. R. Mizell, and O. W. Day, Int. J. Quantum Chem. **57**, 355 (1996).
[52] S. Patchkovskii, Z. Zhao, T. Brabec, and D. M. Villeneuve, Phys. Rev. Lett. **97**, 123003 (2006).
[53] C. G. Ning, X. G. Ren, J. K. Deng, G. L. Su, S. F. Zhang, S. Knippenberg, and M. S. Deleuze, Chem. Phys. Lett. **421**, 52 (2006).
[54] R. J. F. Nicholson, I. E. McCarthy, and W. Weyrich, J. Phys. B **32**, 3873 (1999).